ACS APPLIED MATERIALS & INTERFACES

Research Article

www.acsami.org

# *syn*-/*anti*-Anthradithiophene Derivative Isomer Effects on Semiconducting Properties

Masashi Mamada,* Hiroshi Katagiri, Makoto Mizukami, Kota Honda, Tsukuru Minamiki, Ryo Teraoka, Taisuke Uemura, and Shizuo Tokito

Graduate School of Science and Engineering, Yamagata University, Yonezawa, Yamagata 992-8510, Japan

Supporting Information

**ABSTRACT:** Isomerically pure *syn*-/*anti*-anthradithiophene derivatives have been developed in the past few years. Although *anti*-isomers showed higher field-effect mobilities than mixture of isomers have been reported, a detailed comparison of *syn*-isomer and *anti*-isomer molecules has not been carried out. In this study, we took newly synthesized pure unsubstituted *syn*-/*anti*-anthradithiophenes (ADTs) and compared their single crystal structures, physical properties and semiconducting behavior with a previously studied *syn*-/*anti*-dimethylanthradithiophenes (DMADTs). Although the both isomers were typical herringbone packing structures with similar parameters, *anti*-isomers involved less disordered atoms in the crystal packing. The results from thermal analysis, UV−vis spectra, photo luminescence spectra and cyclic voltammograms of *syn*-/*anti*-anthradithiophenes were nearly the in the solid state as well as in solution. However, field-effect transistors showed obvious differences with mobilities of 0.12 $cm^2\ V^{-1}\ s^{-1}$ for *anti*-anthradithiophene and 0.02 $cm^2\ V^{-1}\ s^{-1}$ for *syn*-anthradithiophene. Because the crystallinity of thin-films measured by X-ray diffraction (XRD) and atomic force microscopy (AFM) seems to be better in *syn*-isomers, the differences in transistor performance are likely attributed to local defects affecting intermolecular interactions, such as disorder in the crystal packing and charge−dipole interactions.

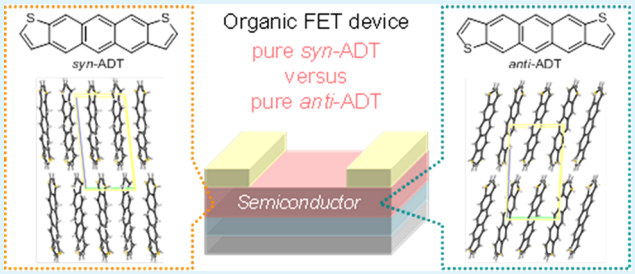


**KEYWORDS:** *organic field-effect transistors, organic semiconductors, thienoacenes, symmetry, crystal structures*

## INTRODUCTION

Thienoacenes have shown excellent promise for use as semiconductors in organic electronic devices such as organic field-effect transistors (OFETs).[1−8] In particular, anthradithiophene (ADT) is isoelectronic with pentacene which is the most researched semiconducting material in OFETs, and a number of pentacene analogues have been also developed.[9−20] ADT was originally synthesized as the mixture of *syn*-isomer and *anti*-isomer due to a difficulties with isomer separation.[21,22] Recently, isomerically pure ADT derivatives were synthesized by developing new synthetic paths for *syn*-isomers[23,24] and *anti*-isomers,[25,26] respectively. Pure *syn*-ADTs substituted with trialkyl-silylethynyl groups at 5,11-positions (*peri*-position), which is the direction of the short molecular axis, showed similar field-effect mobilities to the mixture of isomers.[24] Because the corresponding *anti*-isomers have not been synthesized, it is difficult to conclude that both *syn*-/*anti*-isomers have slight differences in OFET devices. However, *anti*-isomers with/without substituents in the long molecular axis showed superior mobilities compared to the mixture of isomers.[26] Because the obtained materials were limited to *anti*-isomers, a comparison of *syn*-isomers with *anti*-isomers was not possible. Therefore, an improved understanding is required of the isomer effects on the OFET characteristics through the direct comparison of *syn*-/*anti*-isomers, even though a set of corresponding pure isomers are scarce and difficult to obtain.

One strategy for the isolation of isomers is a separation of mixed products by taking advantages of a difference in dipole moment derived from the bulky substituents.[27,28] However, large differences in the molecular shape by the bulky functional groups would strongly affect a manner of intermolecular interaction and charge transport properties, whereby an essential effect of the isomeric core structure is relatively low. Nevertheless, we have recently developed a novel synthetic method for simple structure of both *syn*-/*anti*-ADT derivatives, whereby 2,8-dimethyl-substituted ADTs were synthesized (Figure 1: *syn*-DMADT as **1** and *anti*-DMADT as **2**).[29] Those compounds showed obvious differences in physical

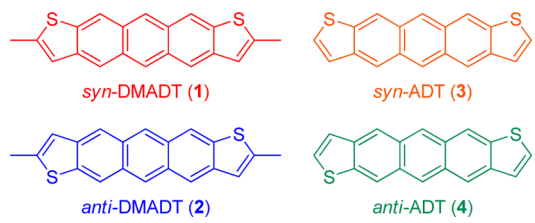


**Figure 1.** ADT Derivatives Structures **1**−**4**.

**Received:** July 9, 2013
**Accepted:** September 12, 2013
**Published:** September 12, 2013

properties in the solid state, in particular, the field-effect mobility of *anti*-DMADT was higher than that of *syn*-DMADT. The same tendency has been seen in naphthodithiophene (NDT) derivatives.[30] In addition, the importance of possessing a $C_2$ symmetry was suggested with an axis perpendicular to the conjugation plane, whose molecule contains an inversion center, in order to achieve a uniform molecular packing in polymers and resulting in high mobilities in a previous report.[31] Because *syn*-ADTs are noncentrosymmetric and *anti*-ADTs are centrosymmetric molecules, *anti*-ADTs appear to be favorable, which is consistent with our findings. However, the relationship between symmetry and mobility and what factors most strongly affect the OFET devices are still unclear.

To obtain further insights into the relationship between molecular structure and charge transport properties, we synthesized isomerically pure unsubstituted *syn*-/*anti*-ADT (**3** and **4**), although the *anti*-isomer **4** was previously prepared elsewhere with different synthetic paths in a study involving a comparison with isomerically mixed ADT.[26] In this report, detailed isomer effects are investigated by comparing both *syn*-isomers (**1** and **3**) and *anti*-isomers (**2** and **4**) with X-ray single-crystal analyses, quantum calculations, thermal analyses, UV–vis and photoluminescence spectroscopies, cyclic voltammetry, X-ray diffraction (XRD), atomic force microscope (AFM), and semiconducting properties.

## EXPERIMENTAL SECTION

**General.** Commercially available materials were used as received from the suppliers. Details of instruments and reagents are shown in the Supporting Information. Compounds **3** and **4** were synthesized by modifying reported procedures.[29,32−34]

**Synthesis of 4,6-Di(thiophene-2-carbonyl)isophthalic Acid (3d) and 2,5-Di(thiophene-2-carbonyl)terephthalic Acid (4d) and Their Separation.** Magnesium turnings (1.23 g, 50.7 mmol) were suspended in THF (100 mL) under argon. 2-Bromothiophene (8.28 g, 50.8 mmol) was added slowly dropwise and the mixture was refluxed for 1 h. The generated ThMgBr was allowed to cool to room temperature and transferred to a separate flask containing pyromellitic dianhydride (5.52 g, 25.3 mmol) in THF (100 mL) under argon at 0 °C. The reaction mixture was heated to reflux overnight. After cooling, the reaction was quenched with water followed by adding 1N-HCl. The organic phase was separated and the aqueous phase was extracted with $CHCl_3$/THF (20:1). The combined organic extracts were dried over sodium sulfate and evaporated in vacuo to give a beige solid as a mixture of *meta*-/*para*-isomers (7.96 g, 81%). The *meta*-/*para*-isomers are formed in a ratio of ca. 1:1 determined by NMR spectroscopy. The isomers were separated by taking advantage of the solubility characteristics in 60% acetic acid. The *para*-isomer is little soluble in 60% acetic acid and precipitated on recrystallization. The *meta*-isomer could be obtained from filtrate by removing solvents.

The *meta*-isomer **3d** was isolated as a gray solid (3.65 g, 37%). Mp: 243 °C. $^1$H NMR: $\delta$/ppm (500 MHz, DMSO-$d_6$, $Me_4Si$) = 8.49 (s, 1H); 8.07 (d, 2H, $J$ = 4.8 Hz); 7.66 (s, 1H); 7.39 (d, 2H, $J$ = 3.8 Hz); 7.18 (dd, 2H, $J$ = 3.8 Hz, $J$ = 4.8 Hz). $^{13}$C NMR: $\delta$/ppm (125 MHz, DMSO-$d_6$) = 187.3, 165.7, 143.8, 143.5, 136.0, 135.5, 131.7, 131.2, 128.9, 126.9. MS/FD: $m/z$ 386 ($M^+$, 100%). IR: $\nu_{max}$/cm$^{-1}$ = 2836, 1689, 1659, 1635, 1512, 1495, 1443, 1412, 1355, 1323, 1302, 1289, 1260, 1236, 1167, 1128, 1089, 1069, 1056, 996, 923, 875, 839, 798, 790, 779, 727. Anal. Calcd. For $C_{18}H_{10}O_6S_2$: C, 55.95; H, 2.61; S, 16.60. Found: C, 55.98; H, 2.51; S, 16.46.

The *para*-isomer **4d** was isolated as a colorless solid (3.31 g, 32%). Mp: 318 °C. $^1$H NMR: $\delta$/ppm (500 MHz, DMSO-$d_6$, $Me_4Si$) = 8.12 (d, 2H, $J$ = 4.8 Hz); 7.98 (s, 2H); 7.47 (d, 2H, $J$ = 3.7 Hz); 7.22 (dd, 2H, $J$ = 4.8 Hz, $J$ = 3.7 Hz). $^{13}$C NMR: $\delta$/ppm (125 MHz, DMSO-$d_6$) = 187.3, 165.8, 143.4, 141.6, 136.1, 135.8, 133.3, 129.0, 128.9. MS/FD: $m/z$ 386 ($M^+$, 100%). IR: $\nu_{max}$/cm$^{-1}$ = 2840, 1735, 1692, 1686, 1651, 1514, 1490, 1412, 1373, 1351, 1306, 1262, 1234, 1152, 1124, 1076, 1058, 925, 903, 887, 851, 801, 774, 745. Anal. Calcd. For $C_{18}H_{10}O_6S_2$: C, 55.95; H, 2.61; S, 16.60. Found: C, 56.02; H, 2.42; S, 16.37.

**Synthesis of 4,6-Bis((thiophen-2-ylmethyl)isophthalic Acid (3c) and 2,5-Bis(thiophen-2-ylmethyl)terephthalic Acid (4c).** Each compound (1.97 g, 5.11 mmol of **3d**, 1.55 g, 4.01 mmol of **4d**) was dissolved in concentrated ammonium hydroxide, and zinc powder (20 equiv.) was added. The resulting solution was refluxed for 2 days with an additional concentrated ammonium hydroxide added several times. The cooled reaction mixture was filtered to remove zinc and the filtrate was washed with chloroform several times and acidified with hydrochloric acid. The colorless solid was collected by filtration and washed with water and dried to give each product (1.78 g, 97% of **3c**, 1.44 g, quant. of **4c**) as a colorless solid.

**3c**: Mp: 257 °C. $^1$H NMR: $\delta$/ppm (500 MHz, DMSO-$d_6$, $Me_4Si$) = 13.18 (br, 2H); 8.34 (s, 1H); 7.43 (s, 1H); 7.28 (d, 2H, $J$ = 5.2 Hz); 6.89 (dd, 2H, $J$ = 5.2 Hz, $J$ = 3.4 Hz); 6.79 (d, 2H, $J$ = 3.4 Hz); 4.55 (s, 4H). $^{13}$C NMR: $\delta$/ppm (125 MHz, DMSO-$d_6$) = 167.5, 145.4, 142.9, 134.2, 133.3, 128.1, 126.7, 125.3, 124.5, 32.9. MS/FD: $m/z$ 358 ($M^+$, 100%). IR: $\nu_{max}$/cm$^{-1}$ = 2865, 1676, 1605, 1551, 1420, 1399, 1299, 1283, 1253, 1241, 1120, 1111, 1077, 1038, 916, 897, 852, 815, 773, 751, 728. Anal. Calcd. For $C_{18}H_{14}O_4S_2$: C, 60.32; H, 3.94; S, 17.89. Found: C, 60.35; H, 3.93; S, 17.91.

**4c**: Mp: 294 °C. $^1$H NMR: $\delta$/ppm (500 MHz, DMSO-$d_6$, $Me_4Si$) = 13.30 (br, 2H); 7.78 (s, 2H); 7.29 (d, 2H, $J$ = 5.2 Hz); 6.90 (dd, 2H, $J$ = 5.2 Hz, $J$ = 3.3 Hz); 6.82 (d, 2H, $J$ = 3.3 Hz); 4.51 (s, 4H). $^{13}$C NMR: $\delta$/ppm (125 MHz, DMSO-$d_6$) = 168.0, 143.3, 139.5, 133.1, 132.8, 126.8, 125.4, 124.6, 32.4. MS/FD: $m/z$ 358 ($M^+$, 100%). IR: $\nu_{max}$/cm$^{-1}$ = 2859, 1692, 1672, 1500, 1430, 1405, 1299, 1270, 1248, 1200, 1174, 1128, 1075, 1037, 921, 846, 820, 812, 799, 762, 743, 707. Anal. Calcd. For $C_{18}H_{14}O_4S_2$: C, 60.32; H, 3.94; S, 17.89. Found: C, 60.54; H, 3.83; S, 17.65.

**Synthesis of (4,6-Bis(thiophen-2-ylmethyl)-1,3-phenylene)-dimethanol (3b) and (2,5-Bis(thiophen-2-ylmethyl)-1,4-phenylene)-dimethanol (4b).** Into a solution of lithium aluminum hydride (6 equiv) in dry ether, each compound (1.70 g, 4.74 mmol of **3c**, 1.06 g, 2.99 mmmol of **4c**) was added slowly on an ice bath. The reaction mixture was stirred at room temperature overnight. It was then quenched by cautiously adding water and enough 10% hydrochloric acid to dissolve the inorganic salts. The organic phase was collected and aqueous phase was extracted with chloroform. The organic phase was washed with water and dried over sodium sulfate and evaporated. The residue was purified by column chromatography on a silica gel using ethyl acetate to give each product (1.22 g, 78% of **3b** as a beige solid, 0.96 g, 99% of **4b** as a gray solid). The $R_f$ values of each isomer on silica gel 60 F254 TLC plate were different when eluted with 100% ethyl acetate; $R_f$ (**3b**) = 0.6 and $R_f$ (**4b**) = 0.7.

**3b**: Mp: 98 °C. $^1$H NMR: $\delta$/ppm (500 MHz, $CDCl_3$, $Me_4Si$) = 7.44 (s, 1H); 7.16 (s, 1H); 7.13 (d, 2H, $J$ = 5.1 Hz); 6.90 (dd, 2H, $J$ = 5.1 Hz, $J$ = 3.4 Hz); 6.72 (d, 2H, $J$ = 3.4 Hz); 4.67 (s, 4H); 4.21 (s, 4H); 1.84 (br, 2H). $^{13}$C NMR: $\delta$/ppm (125 MHz, $CDCl_3$) = 144.1, 138.4, 137.8, 132.5, 129.4, 127.2, 125.3, 124.4, 63.2, 33.0. MS/FD: $m/z$ 330 ($M^+$, 100%); 312 ($M-H_2O^+$, 84%). IR: $\nu_{max}$/cm$^{-1}$ = 3223, 2889, 2850, 1735, 1529, 1481, 1432, 1404, 1366, 1359, 1292, 1233, 1218, 1110, 1072, 1043, 1035, 1006, 998, 984, 897, 848, 820, 781, 760. Anal. Calcd. For $C_{18}H_{18}O_2S_2$: C, 65.42; H, 5.49; S, 19.41. Found: C, 65.75; H, 5.66; S, 19.34.

**4b**: Mp: 138 °C. $^1$H NMR: $\delta$/ppm (500 MHz, $CDCl_3$, $Me_4Si$) = 7.30 (s, 2H); 7.14 (d, 2H, $J$ = 5.1 Hz); 6.91 (dd, 2H, $J$ = 5.1 Hz, $J$ = 3.5 Hz); 6.74 (d, 2H, $J$ = 3.5 Hz); 4.69 (s, 4H); 4.24 (s, 4H). $^{13}$C NMR: $\delta$/ppm (125 MHz, $CDCl_3$) = 144.0, 138.7, 137.4, 130.8, 127.2, 125.4, 124.4, 63.3, 32.9. MS/FD: $m/z$ 330 ($M^+$, 100%). IR: $\nu_{max}$/cm$^{-1}$ = 3300, 3204, 2920, 2851, 1737, 1496, 1456, 1436, 1407, 1362, 1279, 1260, 1232, 1187, 1127, 1109, 1072, 1040, 1004, 983, 900, 847, 818, 747. Anal. Calcd. For $C_{18}H_{18}O_2S_2$: C, 65.42; H, 5.49; S, 19.41. Found: C, 66.35; H, 5.38; S, 19.20.

**Synthesis of 4,6-Bis(thiophen-2-ylmethyl)-isophthalaldehyde (3a) and 2,5-Bis(thiophen-2-ylmethyl)-terephthalaldehyde (4a).** A solution of each compound (1.22 g, 3.69 mmol of **3b**, 0.828 g, 2.51 mmol of **4b**) in dry pyridine was added slowly to a suspension of chromium(VI) oxide (10 equiv) and dry

**Scheme 1. Synthesis of 3 (*syn*-ADT) and 4 (*anti*-ADT)**

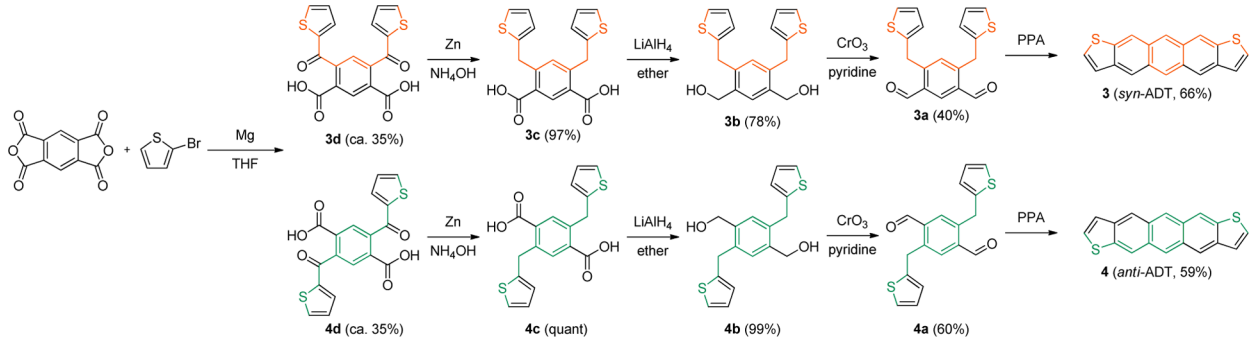


pyridine. After stirring 3 h at room temperature, the reaction mixture was filtered and washed with chloroform. The filtrate was washed with 10% hydrochloric acid and 10% sodium carbonate solution successively. The organic phase was dried over sodium sulfate and evaporated. The residue was purified by column chromatography on a silica gel using dichloromethane to give each product (0.480 g, 40% of **3a** as yellow oil, 0.487 g, 60% of **4a** as a yellow solid).

**3a**: $^1$H NMR: $\delta$/ppm (500 MHz, $CDCl_3$, $Me_4Si$) = 10.27 (s, 2H); 8.32 (s, 1H); 7.33 (s, 1H); 7.16 (d, 2H, $J$ = 5.2 Hz); 6.91 (dd, 2H, $J$ = 5.1 Hz, $J$ = 3.4 Hz); 6.77 (d, 2H, $J$ = 3.4 Hz); 4.64 (s, 4H). $^{13}$C NMR: $\delta$/ppm (125 MHz, $CDCl_3$) = 191.2, 148.2, 141.8, 137.6, 134.6, 133.0, 127.4, 126.3, 125.0, 33.0. MS/FD: $m/z$ 326 ($M^+$, 39%); 308 ($M-H_2O^+$, 100%). IR: $\nu_{max}$/cm$^{-1}$ = 3107, 2860, 2752, 1692, 1603, 1559, 1437, 1419, 1403, 1380, 1360, 1325, 1298, 1236, 1174, 1110, 1076, 1060, 1039, 910, 850, 828, 792. Anal. Calcd. For $C_{18}H_{14}O_2S_2$: C, 66.23; H, 4.32; S, 19.65. Found: C, 66.58; H, 4.18; S, 19.47.

**4a**: Mp: 117 °C. $^1$H NMR: $\delta$/ppm (500 MHz, $CDCl_3$, $Me_4Si$) = 10.29 (s, 2H); 7.81 (s, 2H); 7.17 (d, 2H, $J$ = 5.2 Hz); 6.92 (dd, 2H, $J$ = 5.2 Hz, $J$ = 3.5 Hz); 6.77 (d, 2H, $J$ = 3.5 Hz); 4.64 (s, 4H). $^{13}$C NMR: $\delta$/ppm (125 MHz, $CDCl_3$) = 191.8, 142.4, 141.5, 137.1, 135.0, 127.4, 126.1, 124.9, 32.3. MS/FD: $m/z$ 326 ($M^+$, 100%). IR: $\nu_{max}$/cm$^{-1}$ = 3111, 2848, 1688, 1486, 1434, 1419, 1411, 1354, 1316, 1283, 1261, 1208, 1180, 1121, 1078, 1039, 1004, 937, 854, 812, 773, 750, 743, 717, 707. Anal. Calcd. For $C_{18}H_{14}O_2S_2$: C, 66.23; H, 4.32; S, 19.65. Found: C, 66.14; H, 4.24; S, 19.38.

**Synthesis of Anthra[2,3-*b*:7,6-*b*′]dithiophene (3) and Anthra[2,3-*b*:6,7-*b*′]dithiophene (4).** A mixture of each compound (0.405 g, 1.24 mmol of **3a**, 0.219 g, 0.671 mmol of **4a**) and 10 g of polyphosphoric acid (PPA) was heated to 85 °C for 30 min. After cooling, ice water was added to the reaction mixture and the precipitated reddish brown solid was collected by filtration and washed with methanol. After drying, the crude product was purified by sublimation to give each product (0.239 g, 66% of **3** as an orange solid, 0.114 g, 59% of **4** as an orange solid).

**3** (*syn*-isomer): Decomposition (5% weight loss) temperature: 430 °C. Mp: 454 °C. MS/FD: $m/z$ 290 ($M^+$, 100%). IR: $\nu_{max}$/cm$^{-1}$ = 3062, 1736, 1685, 1516, 1403, 1395, 1312, 1277, 1241, 1159, 1076, 1031, 1022, 1005, 903, 832, 825, 805, 733. Anal. Calcd. For $C_{18}H_{10}S_2$: C, 74.45 H, 3.47; S, 22.08. Found: C, 74.58; H, 3.44; S, 22.14.

**4** (*anti*-isomer): Decomposition (5% weight loss) temperature: 433 °C. Mp: 457 °C. MS/FD: $m/z$ 290 ($M^+$, 100%). IR: $\nu_{max}$/cm$^{-1}$ = 3065, 1743, 1685, 1610,1529, 1509, 1396, 1388, 1337, 1306, 1277, 1247, 1129, 1078, 1000, 903, 867, 834, 821, 799, 746, 729, 714. Anal. Calcd. For $C_{18}H_{10}S_2$: C, 74.45 H, 3.47; S, 22.08. Found: C, 74.70; H, 3.43; S, 22.36.

**Device Fabrications.** The HMDS (hexamethyldisilazane) treatment was carried out by immersing the substrate in HMDS at room temperature for >10 h. The ODTS (octadecyltrichlorosilane) treatment was carried out by immersing the substrate in 2 vol % ODTS in toluene at 60 °C for 30 min. PS (polystyrene) was spin-coated from 0.5 wt % xylene solution at the rotational speed of 500 rpm for 5 s, and then 4000 rpm for 120 s. OFETs were constructed on heavily doped n-type silicon wafers covered with thermally grown silicon dioxide (200 nm) which was cleaned by piranha solution. The silicon dioxide acts as a gate dielectric layer, and the silicon wafer serves as a gate electrode. Organic semiconductors (50 nm) were deposited on the silicon dioxide by vacuum evaporation at a rate of 0.2−0.3 Å s$^{-1}$ under pressure of 1 × 10$^{-5}$ Pa. During the evaporation, the temperature of the substrate was maintained to room temperature. Gold was used as source and drain electrodes (50 nm) and deposited on the oraganic semiconductor layer through a shadow mask with $L/W$ = 70/1000 $\mu$m. The FET measurements were carried out at room temperature in a glovebox without exposure to air with a semiconductor parameter analyzer (4200-SCS, KEITHLEY). Mobilities ($\mu$) were calculated in the saturation regime by the relationship: $\mu_{sat} = (2I_DL)/[WC_{ox}(V_G - V_{th})^2]$ where $I_D$ is the source−drain saturation current, $C_{ox}$ (4 F) is the oxide capacitance, $V_G$ is the gate voltage, and $V_{th}$ is the threshold voltage. The latter can be estimated as the intercept of the linear section of the plot of $V_G$ $(I_D)^{1/2}$.

## RESULTS AND DISCUSSION

**Isomer Synthesis.** The synthesis of isomers **3** and **4** were performed in accordance with the synthesis of isomers **1** and **2** as shown in Scheme 1. The first step in the reaction was changed from the previous method, although the procedures in the later steps were nearly same.[29] The Grignard reaction using bromothiophene was selected instead of the Friedel−Crafts acrylation of thiophene rings to prevent a second reaction of the thiophene ring by electrophilic species, which was excluded in the previously used methylthiophene. The ratio of obtained *meta*-isomer **3d** and *para*-isomer **4d** was approximately 1:1, which is different from the 2:1 ratio of compounds **1d** and **2d** derived by the Friedel−Crafts reaction for methyl-substituted compounds of **3d** and **4d**, respectively. Although compounds **1d** and **2d** were successfully separated by recrystallization from glacial acetic acid, followed by precipitation of *para*-isomer **2d** and evaporation of the filtrate for *meta*-isomer **1d**, the same conditions could not be reached because the solubility of isomers **3d** and **4d** were higher, that is, *para*-isomer **4d** did not precipitate in the glacial acetic acid. Therefore, the solubility of the products was modulated (reduced) by adding water, and 60% acetic acid gave better results for the precipitation of isomer **4d**. Subsequently, compounds **3b** and **4b** in their third steps could be purified by column chromatography with different $R_f$ values, resulting in high isomeric purity. The final ring closing reaction with polyphosphoric acid (PPA) gave isomerically pure compounds **3** and **4** with good yields. The products were fully characterized by X-ray single-crystal structure analyses and elemental analyses.

**Single-Crystal Analyses.** The single crystals obtained by vacuum sublimation have validated the molecular geometry of the isomers, that is, isomer **3** crystallizes in the non-centrosymmetric $P1$ which can be solved in the higher symmetry space group $P$-1 with pseudo center of symmetry,


dx.doi.org/10.1021/am4027136 | ACS Appl. Mater. Interfaces 2013, 5, 9670−9677

and isomer **4** belongs to the centrosymmetric *P*-1 space group (Figure 2). Because the molecular shape of isomers **3** and **4** are

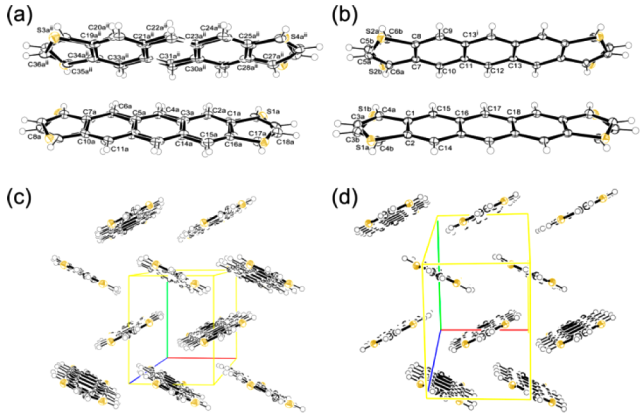


**Figure 2.** Single-crystal structure of (a) isomer **3** and (b) isomer **4**. Packing structure of (c) isomer **3** and (d) isomer **4** (thermal ellipsoids of 50% probability).

quite similar, the packing structures are also similar, with a herringbone motif at a tilt angle of 53.0° for isomer **3** and 51.8° for isomer **4**. There are two independent molecules in the asymmetric units within both crystals. All molecules involve crystal disorder. Although the disorder of *syn*-isomer **3** spans the whole range of molecules in approximately 50/50 occupancies, *anti*-isomer **4** has major and minor conformers, whereby molecules 1A and 1B is 68:32 and molecules 2A and 2B is 90:10. In addition, disorder in isomer **4** occurred only at thiophene ring portions of molecules. Therefore, most of the region of orbital overlaps for charge transportation in **4** is located in ordered (undisordered) anthracene cores. In the case of DMADT, *syn*-isomer **1** was disordered, whereas no disorder was found in *anti*-isomer **2**. Thus, *syn*-isomers of ADTs tend to be disordered and *anti*-isomers have the advantage of a homogeneous orientation.

**Computational Chemistry.** DFT calculations were carried out on the isomers at the B3LYP/6-31G(d,p) level to determine the highest occupied molecular orbitals (HOMOs) and the lowest unoccupied molecular orbitals (LUMOs), and to estimate the intramolecular reorganization energy for hole formation ($\lambda_h$).[35] We found that there was little difference of HOMO−LUMO energies for isomers. As listed in Table 1, the reorganization energies of isomers **1**−**4** were 96.2, 98.7, 91.7, and 94.3 meV, respectively, which are similar and comparable to pentacene (89.3 meV). Unsubstituted ADTs showed smaller values than DMADTs as expected. In addition, the reorganization energies of the *syn*-isomers are slightly smaller than those of the *anti*-isomers. This tendency is consistent with reported values.[36] It is generally known that a smaller reorganization energy and larger intermolecular transfer integral are preferable for charge transport.[37−39] Therefore, the transfer integrals were also calculated at the PW-91/TZP level using the Amsterdam Density Functional (ADF) program package.[40−42] Because the crystals of isomers **3** and **4** contain two independent molecules with crystal disorder, the calculations are complicated and there are some variations at the same positional relationship. The transfer integrals along the stacking and transverse directions are summarized in Table 1 and Figure S3 in the Supporting Information. The transfer integrals of *syn*-isomers tend to be large compared to those of *anti*-isomers.

**Table 1. Calculated Reorganization Energies and Transfer Integrals of ADT Derivatives with the Herringbone Packing Structure in the Solid State**

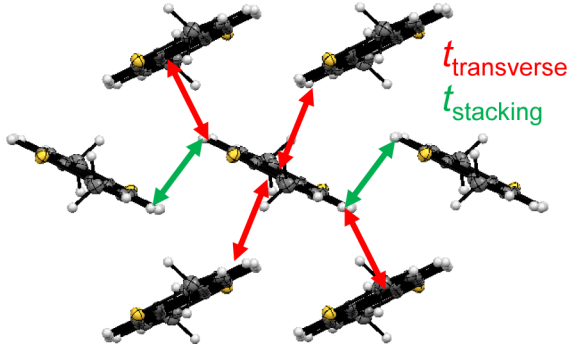


| compd | $\lambda_h$ (meV)[a] | $t_{transverse}$ (meV)[b] | $t_{stacking}$ (meV)[b] |
|---|---|---|---|
| **1**[c] | 96.2 | 12.6−65.7 | 0.4−23.7 |
| **2**[c] | 98.7 | 38.3 | 3.9 |
| **3** | 91.7 | 46.7−91.7 | 33.2−42.0 |
| **4** | 94.3 | 10.2−77.4 | 1.1−16.1 |

[a]Calculated by DFT methods at the B3LYP/6-31G(d,p) level using the Gaussian 09 program. [b]Calculated at the PW-91/TZP level using the ADF program. [c]Crystal data are available in ref 29.

Note that molecules with disorder are subject to strain structures and the overlaps between the molecular orbitals may be overestimated. However, these results indicate advantages for *syn*-isomers in hole transport.

**Thermal Analyses.** Thermogravimetric (TG) and differential scanning calorimetric (DSC) analyses of isomers **3** and **4** were also carried out. In past report, obvious differences between the isomers of DMADT (isomers **1** and **2**) in thermal analysis were observed, where *anti*-isomer **2** showed higher temperature for 5% weight losses (440 °C) compared to *syn*-isomer **1** (424 °C). In contrast, isomers **3** and **4** showed little differences, as shown in Figure 3. The 5% weight losses were at

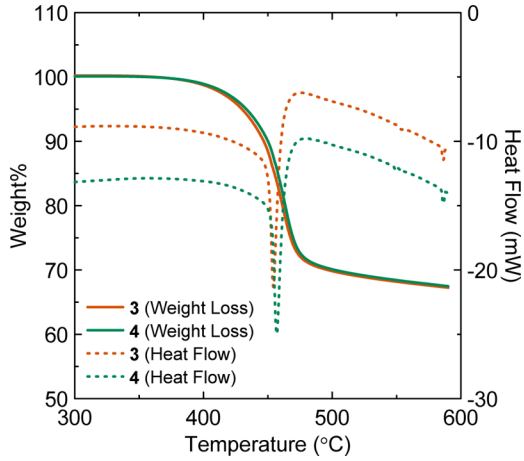


**Figure 3.** TG and DSC analyses for isomers **3** and **4**.

temperatures of 430 and 433 °C for isomers **3** and **4**, respectively. Similar to DMADT isomers **1** and **2**, the *anti*-isomer exhibited higher temperatures, suggesting stronger intermolecular interactions. The minimal difference between isomers is attributed to similar molecular shape and crystal packing of isomers **3** and **4**.


dx.doi.org/10.1021/am4027136 | ACS Appl. Mater. Interfaces 2013, 5, 9670−9677

**UV–Vis and PL Spectra.** The UV–vis spectra in dichloromethane and a 50 nm thin film on quartz are shown in Figure 4. The lowest energy maxima of isomers **3** and **4** were

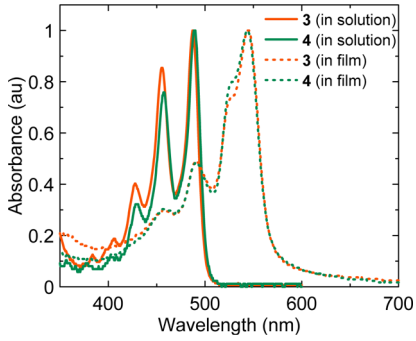


**Figure 4.** Normalized absorption spectra of isomers **3** and **4** in $CH_2Cl_2$ (solid line) and in film form (dashed line).

489 and 488 nm in solution, and 545 and 544 nm in the film, respectively. A 1 nm red shift of the absorption maximum for *syn*-isomer in solution is the same as DMADT isomer **1** and **2**. Although a clear difference was observed in the absorption of isomer **1** and **2** in film form, the absorption of isomer **3** and **4** films is nearly the same, which have the same tendency as results from thermal analyses and photoluminescence spectra for isomers **1**–**4** (see Figure S4 in the Supporting Information). In other words, the *syn*-/*anti*-isomers in solution have similar properties and the unsubstituted *syn*-/*anti*-ADT isomers **3** and **4** showed slight differences even in film form, although films for *syn*-/*anti*-DMADT isomers **1** and **2** showed obvious differences.

**Cyclic Voltammetry.** Similar to the optical measurements, the electrochemical measurements of isomers **3** and **4** exhibited nearly the same results. The cyclic voltammograms of isomers **3** and **4** showed reversible oxidation and reduction peaks, as shown in Figure 5. The first oxidation potentials of isomers **3**

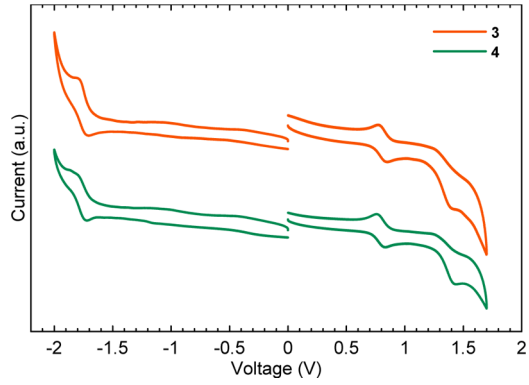


**Figure 5.** Cyclic voltammetry measurements for isomers **3** and **4** in *o*-dichlorobenzene at 100 °C vs Ag/AgCl ($Fc/Fc^+$ = 0.49 V).

and **4** were 0.30 and 0.30 V in solution and 0.41 and 0.40 V in film form vs $Fc/Fc^+$, respectively. These were shifted to the positive direction from the oxidation potentials of isomers **1** and **2** (0.23 V vs $Fc/Fc^+$ in solution) due to the lack of electron donating alkyl groups. The electrochemically derived HOMO–LUMO energy gaps are 2.51 eV for isomers **3** and **4**, which is consistent with optical energy gaps (2.48 eV for isomer **3** and 2.47 eV for isomer **4**). These results are summarized in Table 2.

**Table 2. Photophysical and Electrochemical Properties for Isomers 3 and 4**

| | compd | $\lambda_{abs}$ (nm)[a] | $E_{ox1}$ (V)[b] | $E_{ox2}$ (V)[b] | $E_{red}$ (V)[b] | HOMO (eV)[c] | LUMO (eV)[c] |
|---|---|---|---|---|---|---|---|
| **3** | solution | 488 | 0.30 | 0.87 | −2.21 | −5.10 | −2.59 |
| | calcd[d] | 498 | | | | −4.81 | −2.01 |
| | film | 545 | 0.41 | 0.94 | −1.52 | −5.21 | −3.28 |
| **4** | solution | 489 | 0.30 | 0.87 | −2.21 | −5.10 | −2.59 |
| | calcd[d] | 499 | | | | −4.81 | −2.02 |
| | film | 544 | 0.40 | 0.92 | −1.51 | −5.20 | −3.29 |

[a]The lowest energy maxima. [b]Determined by differential pulse voltammetry measurement in a 0.1 M solution of $Bu_4NPF_6$ in *o*-dichlorobenzene at 100 °C or in film form with 0.1 M solution of $Bu_4NPF_6$ in $CH_2Cl_2$ at rt (vs $Fc/Fc^+$). [c]Estimated vs vacuum level from $E_{HOMO} = -4.80 - E_{ox}$ or $E_{LUMO} = -4.80 - E_{red}$. [d]Calculated by DFT methods at the B3LYP/6-31G(d,p) level using Gaussian 09 program.

**XRD and AFM Measurements.** Thin film morphologies that affect charge carrier transport were examined using X-ray diffraction (XRD) and atomic force microscopy (AFM) for isomers **1**–**4**. The XRD analyses and AFM images for thin films of each isomer were deposited on HMDS-treated $SiO_2$ substrates, as shown in Figure 6. In comparing *syn*-isomers (Figure 6a, c) and *anti*-isomers (Figure 6b, d), *syn*-isomers may have a higher level of crystallinity, which benefits carrier transport. The observed XRD peaks for *syn*-isomers **1** and **3** showed stronger intensities, higher-order reflections and narrower full width at half-maximum (FWHM) than those for the *anti*-isomers **2** and **4**. In addition, AFM images of *syn*-isomers exhibited larger grain sizes, which generally contribute to increased carrier mobility, supporting the XRD results. Therefore, the thin-films of *syn*-isomers appear to more appropriate for OFET devices. These tendencies in film morphology between *syn*-/*anti*-isomers have also been observed in NDT derivatives, whereby *syn*-isomers thin films exhibit larger crystal grains and higher XRD intensities.[30]

The *d*-spacing obtained from the first reflection peak of the out-of-plane XRD for isomers **1**–**4** were 17.6 Å ($2\theta$ = 5.03°) for isomer **1**, 16.8 Å ($2\theta$ = 5.25°) for isomer **2**, 14.5 Å ($2\theta$ = 6.10°) for isomer **3**, and 14.3 Å ($2\theta$ = 6.18°) for isomer **4**, respectively, which are longer than the molecular lengths (15.6 Å for DMADTs and 13.7 Å for ADTs) obtained from the single-crystal analyses. Therefore, these molecules appear to form lamellar ordering on the substrate. Because the *c*-axis of a unit cell for the single crystal, which is the direction of the long axis of molecules, are 14.4 Å for isomer **3** and 14.0 Å for isomer **4**, these thin-films represent single crystalline packing structures. The in-plane XRD measurements for films 50 nm thick (Figure 6) are also well-indexed by a crystallographic cell. Moreover, in-plane XRD measurements of thinner films (~5 nm) for **3** and **4** showed nearly the same reflections as those of the 50 nm films (see Figure S8 in the Supporting Information). Therefore, molecular orientations near the substrate, which govern charge transport properties, have a single-crystalline phase. For this reason, the results from the bulk single-crystal measurements and the ADF calculations may correlate with OFET device performance.

**Field-Effect Transistors.** OFET devices based on isomers **3** and **4** were fabricated with a top-contact TFT construction. Figure 7 shows the electrical transfer and output characteristics of the devices fabricated on an HMDS-treated substrate. The TFT devices of both isomers **3** and **4** showed typical p-type

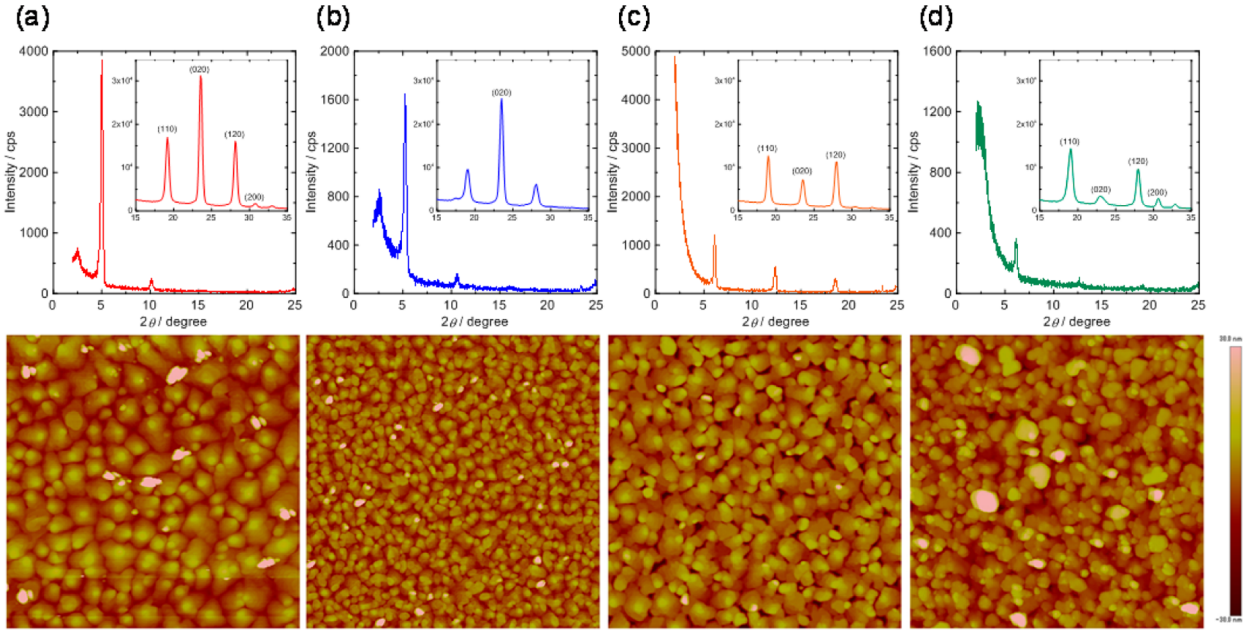


**Figure 6.** Out-of-plane and in-plane (insets) X-ray diffractograms and AFM images (5 $\mu$m × 5 $\mu$m) of 50 nm thin films of (a) isomer **1**, (b) isomer **2**, (c) isomer **3**, and (d) isomer **4** deposited on HMDS-treated $SiO_2$ at room temperature.

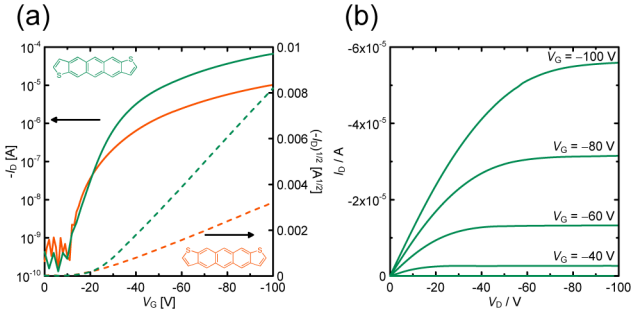


**Figure 7.** (a) Transfer characteristics for isomer **3** (orange) and isomer **4** (green), and (b) output characteristics for isomer **4** deposited on the HMDS-treated $SiO_2$ at rt.

behavior, whereby differences that depend on the core structures between isomers was observed, as in DMADTs. In the transfer curves, the rising edge of $I_D$ ($V_{on}$) were nearly the same for both *syn*-/*anti*-isomers due to the similar HOMO levels of isomers **3** and **4**, although the levels were somewhat shifted to higher potentials compared with those of DMADT devices **1** and **2**. This resulted in similar electrode-semiconductor carrier injection properties for each isomer. However, the on-currents were clearly different between isomers **3** and **4**. As a result, the mobilities of the isomers were estimated be sufficient to account for the differing carrier transport properties. The mobility of *syn*-isomer **3** was 0.012 $cm^2\ V^{-1}\ s^{-1}$, whereas *anti*-isomer **4** showed a significantly higher mobility of 0.12 $cm^2\ V^{-1}\ s^{-1}$. The reported mobility for a mixture of isomers was 0.01 $cm^2\ V^{-1}\ s^{-1}$, which is a rather low compared to the mobility of the *syn*-isomer.[22] Devices fabricated on ODTS-treated substrates showed slightly improved mobilities for both isomers despite being amorphous layers (see Figure S6 in the Supporting Information). Here, the mobilities of *anti*-isomer **4** were also 1 order of magnitude higher than those of *syn*-isomer **3**. These results validate the importance of separating the isomers as found in previous reports on DMADT and NDT derivatives,[29,30] and that *anti*-isomers are generally better as semiconductor in OFETs than *syn*-isomers.

Our interest is how structural differences in isomers affect field-effect mobility levels. Here, isomers **3** and **4** are both isoelectronic forms of pentacene. Thus, the physical properties measured in solution are quite similar, although the *syn*-isomers possess slightly lower reorganization energies, favorable for charge transport. For DMADTs, the molecular shape of *syn*-/*anti*-isomers were slightly different due to the methyl substituents, resulting in distinct intermolecular interactions as seen in the single crystal analyses and dissimilar optical properties for the layers. In contrast, isomers **3** and **4** have nearly the same molecular shape, affording a similar packing motif and the optical/electrochemical properties in the layers. However, these properties are not identical as a matter of course, and the differences were more clearly seen by XRD in the crystallinity of thin-films and the result of calculations for intermolecular orbital overlaps, reflecting different intermolecular interactions.

These data showed a comparable advantage of *syn*-isomers in charge transport. Unfortunately, these issues could not account for a marked superiority of *anti*-isomers in actual OFET devices. A likely explanation is that more homogeneous orientations, supported by the crystal structures with less disorder in *anti*-isomers, decreases a formation of potential charge carrier trap sites in the channel region. Besides this, *syn*-isomer dipoles are considered important for the local interactions between molecules, although the dipole moments are averaged within the deposited layer. Centrosymmetric compounds such as *anti*-isomers do not have permanent dipole moments, whereas *syn*-isomers, which are axisymmetric molecules, have dipole moments in the direction of the short molecular axis. When a hole injected into the molecule for carrier transport, the adjacent molecules with a dipole moment undergo a reorientation, which is the energy loss during intermolecular relaxation, decreasing charge carrier mobility. Molecules having permanent dipole moments are subject to influence more than molecules without dipoles. In essence, the


dx.doi.org/10.1021/am4027136 | ACS Appl. Mater. Interfaces 2013, 5, 9670−9677

symmetry of molecules strongly, even for molecules with the same shape, affects the field-effect mobility; it is critically important to consider this in order to achieve a high mobility levels.

**Table 3. OFET Characteristics for Isomers 3 and 4**

| compd | condition | $\mu$ ($cm^2\ V^{-1}\ s^{-1}$) | on/off ratio | threshold $V_{th}$ (V) |
|---|---|---|---|---|
| 3 | HMDS | 0.012 | $1 \times 10^4$ | −20 |
| | ODTS | 0.017 | $1 \times 10^4$ | −17 |
| 4 | HMDS | 0.12 | $1 \times 10^4$ | −21 |
| | ODTS | 0.18 | $1 \times 10^5$ | −20 |

Finally, we fabricated the devices for DMADT isomers **1** and **2** under different conditions because the mobilities of DMADTs in the past report, where 0.084 $cm^2\ V^{-1}\ s^{-1}$ for isomer **1** and 0.41 $cm^2\ V^{-1}\ s^{-1}$ for isomer **2** were obtained with HMDS surface treatments, were better than those of ADTs. Unlike with ADTs, the ODTS treatments did not lead to improvements in mobility as compared to HMDS treatments. The mobilities of the devices on an ODTS-treated substrate were 0.013 $cm^2\ V^{-1}\ s^{-1}$ for isomer **1** and 0.12 $cm^2\ V^{-1}\ s^{-1}$ for isomer **2**. On the other hand, the devices on polystyrene-coated silicon substrates showed the similar mobilities to the HMDS-treated devices. The mobility of *anti*-isomer **2** was 0.42 $cm^2\ V^{-1}\ s^{-1}$. In all cases, *anti*-isomers exhibited higher charge carrier mobility vs *syn*-isomers.

## CONCLUSION

In this study, we investigated the relationship between molecular structure and field-effect mobility in isomers of ADT derivatives. The devices using *anti*-isomers with inversion centers showed higher electrical performances than axisymmetric *syn*-isomers and a mixture of isomers. The physical properties for each isomer in both solution and film form were only slightly different, which does not enough to explain the large differences in charge transport behavior between the OFET devices. Meanwhile, thin-film morphologies appears be advantageous in *syn*-isomers. Therefore, device performance is felt to be influenced more local intermolecular interactions, where crystal disorder and the charge-dipole interactions that develop in axisymmetric compounds may reduce performance in the OFET devices. These results strongly support centrosymmetry as an important factor in molecular design for OFET materials.

## ASSOCIATED CONTENT

### Supporting Information

Full experimental details, characterization data, and crystallographic information (CIF) files for **3** and **4**. This material is available free of charge via the Internet at http://pubs.acs.org.

## AUTHOR INFORMATION

### Corresponding Author

*E-mail: mamada@yz.yamagata-u.ac.jp.

### Notes

The authors declare no competing financial interest.

## ACKNOWLEDGMENTS

We thank Prof. C. Shepherd and Dr. T. Sakanoue for helpful discussions. This work was financially supported by the Japan Regional Innovation Strategy Program by the Excellence (creating international research hub for advanced organic electronics) of Japan Science and Technology Agency (JST), by the Ministry of Education, Culture, Sports, Science and Technology, Japan, and the UBE foundation.

## REFERENCES

(1) Takimiya, K.; Shinamura, S.; Osaka, I.; Miyazaki, E. *Adv. Mater.* **2011**, *23*, 4347−4370.
(2) Takimiya, K.; Nakano, M.; Kang, M. J.; Miyazaki, E.; Osaka, I. *Eur. J. Org. Chem.* **2013**, 217−227.
(3) Nakano, M.; Mori, H.; Shinamura, S.; Takimiya, K. *Chem. Mater.* **2012**, *24*, 190−198.
(4) Jurchescu, O. D.; Subramanian, S.; Kline, R. J.; Hudson, S. D.; Anthony, J. E.; Jackson, T. N.; Gundlach, D. J. *Chem. Mater.* **2008**, *20*, 6733−6737.
(5) Payne, M. M.; Parkin, S. R.; Anthony, J. E.; Kuo, C.-C.; Jackson, T. N. *J. Am. Chem. Soc.* **2005**, *127*, 4986−4987.
(6) Subramanian, S.; Park, S. K.; Parkin, S. R.; Podzorov, V.; Jackson, T. N.; Anthony, J. E. *J. Am. Chem. Soc.* **2008**, *130*, 2706−2707.
(7) Jurchescu, O. D.; Hamadani, B. H.; Xiong, H. D.; Park, S. K.; Subramanian, S.; Zimmerman, N. M.; Anthony, J. E.; Jackson, T. N.; Gundlach, D. J. *Appl. Phys. Lett.* **2008**, *92*, 132103.
(8) Mei, Y.; Loth, M. A.; Payne, M.; Zhang, W.; Smith, J.; Day, C. S.; Parkin, S. R.; Heeney, M.; McCulloch, I.; Anthopoulos, T. D.; Anthony, J. E.; Jurchescu, O. D. *Adv. Mater.* **2013**, *25*, 4352−4357.
(9) Kelley, T. W.; Muyres, D. V.; Baude, P. F.; Smith, T. P.; Jones, T. D. *Mater. Res. Soc. Symp. Proc.* **2003**, *771*, 169−179.
(10) Anthony, J. E.; Eaton, D. L.; Parkin, S. R. *Org. Lett.* **2002**, *4*, 15−18.
(11) Sheraw, C. D.; Jackson, T. N.; Eaton, D. L.; Anthony, J. E. *Adv. Mater.* **2003**, *15*, 2009−2011.
(12) Swartz, C. R.; Parkin, S. R.; Bullock, J. E.; Anthony, J. E.; Mayer, A. C.; Malliaras, G. G. *Org. Lett.* **2005**, *7*, 3163−3166.
(13) Wang, C.-H.; Jian, S.-D.; Chan, S.-W.; Ku, C.-S.; Huang, P.-Y.; Chen, M.-C.; Yang, Y.-W. *J. Phys. Chem. C* **2012**, *116*, 1225−1231.
(14) Sakanoue, T.; Sirringhaus, H. *Nat. Mater.* **2010**, *9*, 736−740.
(15) Chang, J.-F.; Sakanoue, T.; Olivier, Y.; Uemura, T.; Dufourg-Madec, M. B.; Yeates, S. G.; Cornil, J.; Takeya, J.; Troisi, A.; Sirringhaus, H. *Phys. Rev. Lett.* **2011**, *107*, 066601.
(16) Giri, G.; Verploegen, E.; Mannsfeld, S. C. B.; Atahan-Evrenk, S.; Kim, D. H.; Lee, S. Y.; Becerril, H. A.; Aspuru-Guzik, A.; Toney, M. F.; Bao, Z. *Nature* **2011**, *480*, 504−508.
(17) Tang, M. L.; Okamoto, T.; Bao, Z. *J. Am. Chem. Soc.* **2006**, *128*, 16002−16003.
(18) Valiyev, F.; Hu, W.-S.; Chen, H.-Y.; Kuo, M.-Y.; Chao, I.; Tao, Y.-T. *Chem. Mater.* **2007**, *19*, 3018−3026.
(19) Tang, M. L.; Reichardt, A. D.; Wei, P.; Bao, Z. *J. Am. Chem. Soc.* **2009**, *131*, 5264−5273.
(20) Tang, M. L.; Reichardt, A. D.; Miyaki, N.; Stoltenberg, R. M.; Bao, Z. *J. Am. Chem. Soc.* **2008**, *130*, 6064−6065.
(21) Laquindanum, J. G.; Katz, H. E.; Lovinger, A. J. *J. Am. Chem. Soc.* **1998**, *120*, 664−672.
(22) Chen, M. C.; Kim, C.; Chen, S. Y.; Chiang, Y. J.; Chung, M. C.; Facchetti, A.; Marks, T. J. *J. Mater. Chem.* **2008**, *18*, 1029−1036.
(23) Lehnherr, D.; Hallani, R.; McDonald, R.; Anthony, J. E.; Tykwinski, R. R. *Org. Lett.* **2012**, *14*, 62−65.
(24) Lehnherr, Dan.; Waterloo, A. R.; Goetz, K. P.; Payne, M. M.; Hampel, F.; Anthony, J. E.; Jurchescu, O. D.; Tykwinski, R. R. *Org. Lett.* **2012**, *14*, 3660−3663.
(25) Tylleman, B.; Velde, C. M. L. V.; Balandier, J.-Y.; Stas, S.; Sergeyev, S.; Geerts, Y. H. *Org. Lett.* **2011**, *13*, 5208−5211.
(26) Nakano, M.; Niimi, K.; Miyazaki, E.; Osaka, I.; Takimiya, K. *J. Org. Chem.* **2012**, *77*, 8099−8111.
(27) Li, Z.; Lim, Y.-F.; Kim, J. B.; Parkin, S. R.; Loo, Y.-L.; Malliaras, G. G.; Anthony, J. E. *Chem. Commun.* **2011**, *47*, 7617−7619.
(28) Balandier, J.-Y.; Henry, N.; Arlin, J.-B.; Sanguinet, L.; Lemaur, V.; Niebel, C.; Chattopadhyay, B.; Kennedy, A. R.; Leriche, P.; Blanchard, P.; Cornil, J.; Geerts, Y. H. *Org. Lett.* **2013**, *15*, 302−305.

(29) Mamada, M.; Minamiki, T.; Katagiri, H.; Tokito, S. *Org. Lett.* **2012**, *14*, 4062−4065.
(30) Shinamura, S.; Osaka, I.; Miyazaki, E.; Nakao, A.; Yamagishi, M.; Takeya, J.; Takimiya, K. *J. Am. Chem. Soc.* **2011**, *133*, 5024−5035.
(31) He, M.; Li, J.; Tandia, A.; Sorensen, M.; Zhang, F.; Fong, H. H.; Pozdin, V. A.; Smilgies, D.-M.; Malliaras, G. G. *Chem. Mater.* **2010**, *22*, 2770−2779.
(32) Tedjamulia, M. L.; Tominaga, Y.; Castle, R. N.; Lee, M. L. *J. Heterocycl. Chem.* **1983**, *20*, 1143−1148.
(33) Du, D.; Jiang, Z.; Liu, C.; Sakho, A. M.; Zhu, D.; Xu, L. *J. Organomet. Chem.* **2011**, *696*, 2549−2558.
(34) Mamada, M.; Nishida, J.; Kumaki, D.; Tokito, S.; Yamashita, Y. *J. Mater. Chem.* **2008**, *18*, 3442−3447.
(35) DFT calculations were carried out with Gaussian 09 program package: Frisch, M. J. et al. Gaussian 09, revision C.01; Gaussian, Inc.: Wallingford, CT, 2010; see the Supporting Information for full reference.
(36) Zhang, S.-F.; Chen, X.-K.; Fan, J.-X.; Ren, A.-M. *Org. Electron.* **2013**, *14*, 607−620.
(37) Brédas, J. L.; Beljonne, D.; Coropceanu, V.; Cornil, J. *Chem. Rev.* **2004**, *104*, 4971−5003.
(38) Gruhn, N. E.; da Silva Filho, D. A.; Bill, T. G.; Malagoli, M.; Coropceanu, V.; Kahn, A.; Brédas, J.-L. *J. Am. Chem. Soc.* **2002**, *124*, 7918−7919.
(39) Sakanoue, K.; Motoda, M.; Sugimoto, M.; Sakaki, S. *J. Phys. Chem. A* **1999**, *103*, 5551−5556.
(40) *Amsterdam Density Functional (ADF) Code*, Release 2012; Vrije Universiteit: Amsterdam, The Netherlands, 2012; http://www.scm.com (accessed April 2013).
(41) Senthilkumar, K.; Grozema, F. C.; Bickelhaupt, F. M.; Siebbeles, L. D. A. *J. Chem. Phys.* **2003**, *119*, 9809−9817.
(42) Prins, P.; Senthilkumar, K.; Grozema, F. C.; Jonkheijm, P.; Schenning, A. P. H. J.; Meijer, E. W.; Siebbeles, L. D. A. *J. Phys. Chem. B* **2005**, *109*, 18267−18274.